Journal of Materials Chemistry A

ROYAL SOCIETY OF CHEMISTRY

PAPER

View Article Online
View Journal | View Issue

Cite this: J. Mater. Chem. A, 2021, 9, 27448

Zeolite-driven Ag species during redox treatments and catalytic implications for SCO of NH_3†

Christian W. Lopes, ‡[a] Joaquin Martinez-Ortigosa, [a] Kinga Góra-Marek, [b] Karolina Tarach, [b] José A. Vidal-Moya, [a] Antonio E. Palomares, [a] Giovanni Agostini, [c] Teresa Blasco *[a] and Fernando Rey [a]

Supported silver species are among the most promising catalysts for the depletion of ammonia emission by selective catalytic oxidation (NH_3-SCO). Here, an investigation on the influence of small pore CHA and RHO zeolite structures on the silver species formed and their catalytic activity for the NH_3-SCO reaction has been conducted. To this end, AgRHO(4) and AgCHA(4) zeolites with similar Si/Al molar ratios (≈ 4) and silver content (~15 wt%, Ag/Al ≈ 0.6), and AgCHA(2) with Si/Al ≈ 2 and higher silver loading, while maintaining the Ag/Al ratio (~26 wt%, Ag/Al ≈ 0.6), have been submitted to different treatments and characterized by using a large variety of techniques (XRD, UV-Vis, ^{109}Ag NMR, *in situ* XAS and *operando* FT-IR). The reduction of the AgCHA and AgRHO zeolites at low temperature (100–200 °C) produces silver clusters, which remain in the AgRHO zeolite when the temperature is increased to 400 °C. However, the silver species in the AgCHA zeolites evolve to nanoparticles (NPs) at 400 °C under H_2. The catalytic tests show that metal particles are the active sites while silver clusters are inactive for the NH_3-SCO reaction. Also, there are important differences in the stability of the reduced Ag species under oxidizing or under reaction conditions at 400 °C. Metal NPs are partially redispersed and oxidized to $(Ag)_n^+$, while silver clusters are completely oxidized to Ag^+. Our results indicate that silver clusters are stabilized in the RHO-type and not in the CHA-type zeolite, and thus they display very different catalytic activities for the NH_3-SCO reaction.

Received 9th November 2021
Accepted 22nd November 2021

DOI: 10.1039/d1ta09625g

rsc.li/materials-a

1. Introduction

The development of supported sub-nanometric metal moieties, mainly clusters of few atoms and isolated atomic species, has been the focus of many studies as they can be advantageous from different points of view.[1] In catalysis, the metal dispersion usually increases the activity which, therefore, is expected to improve on small clusters, even if the electronic properties may vary from conventional particles and cause changes in the catalytic behavior. However, the stabilization of metal atoms or clusters may be difficult because of the strong tendency to form large particles (d > 10 nm).[2] An approach to prevent the aggregation of sub-nanometer metal species is their encapsulation within the pores and cavities of microporous materials, as demonstrated for Pt, Pd, Au, Ag, and metal alloys.[3–10] The stabilization of metal clusters in zeolite hosts has been used to exploit their unusual structural, physical, electronic, magnetic, optical and biocidal properties, motivating several studies on their growth and stability under different conditions.[11–14] The diffusion and coalescence of metal moieties depend on the heating temperature and the gases present, and may occur under reaction conditions provoking catalyst deactivation. The inverse path, *i.e.*, the re-dispersion of large metal particles even to isolated atoms by heating under an oxidizing atmosphere, has also been investigated to regenerate deactivated catalysts.[15–17]

Among supported metals, silver is of particular interest because its semi-noble nature facilitates the reduction of the cation to form sub-nanometer metal entities, including stabilized positively charged species and metal nanoparticles (NPs). The ability of silver to modify its aggregation and oxidation states creates incertitude about the chemical species present during any practical application.[14,18–21] For this reason, it is very important to identify the species present in supported silver catalysts submitted to different reduction/oxidation treatments during catalyst optimization for specific processes. Besides this, the framework topology can also control the nature of the silver

[a]*Instituto de Tecnología Química (Universitat Politècnica de València – Consejo Superior de Investigaciones Científicas), Avda. de Los Naranjos s/n, Valencia 46022, Spain. E-mail: tblasco@itq.upv.es*

[b]*Faculty of Chemistry, Jagiellonian University in Kraków, 2 Gronostajowa St., Kraków 30-387, Poland*

[c]*ALBA Synchrotron Light Source, Crta. BP 1413, Km. 3.3, Cerdanyola del Vallès 08290, Spain*

† Electronic supplementary information (ESI) available. See DOI: 10.1039/d1ta09625g

‡ Universidade Federal do Rio Grande do Sul, Instituto de Química, Laboratório de Reatividade e Catálise, Porto Alegre 91501-970, Brazil.

species formed in Ag-zeolite stabilizing clusters and atomically dispersed sites, affecting the catalytic performance. However, the influence of the zeolite structure on the state of silver and the catalytic properties has been scarcely investigated.

The selective catalytic oxidation of ammonia (NH_3-SCO) to N_2 and H_2O is one of the numerous reactions catalyzed by supported noble metals, with Ag-based catalysts, especially Ag/Al_2O_3, being among the most effective catalysts for said reaction.[22–24] The NH_3-SCO is the most promising method for the depletion of ammonia that is recognized as one of the main emerging atmospheric contaminants with detrimental effects on the environment and human health.[25,26] Interest in this process has been increasing in recent years, motivated by the ammonia slip to the atmosphere from the selective catalytic reduction of NO_x (NH_3-SCR-NO_x) and by the more restricting regulations in gas emissions. The SCR units, fitted in heavy-duty diesel vehicles and power plants for the removal of NO_x, use as reducing agent an excess of ammonia, which is generated on-board by urea decomposition.[25,27–29] During this process, NH_3 can be over-oxidized to give other contaminants such as N_2O and NO. Thus, the catalysts must be optimized to enhance N_2 selectivity. In this context, determining the silver species can shed light on the active and selective sites and the reaction pathway, which is assumed to follow the internal SCR (i-SCR) mechanism.[19,29,30] In general, the activity of Ag-supported catalysts increases with the metal dispersion, while the selectivity to N_2 is higher on larger silver particles.[31,32] A previous study of our group indicates that Ag^+ sites in Ag-zeolites are practically inactive for the NH_3-SCO reaction.[33] However, there are still controversies about the role played by charged ($Ag_m^{\delta+}$) and neutral (Ag_n^0) silver clusters, which are usually also present in supported Ag catalysts.

This work focuses on the characterization of the silver species formed in small-pore Ag-zeolites with the CHA and RHO topologies under different reduction/oxidation conditions to determine the influence of the framework structure and with less detail, of the aluminum content of the zeolite host. The effect of thermal treatments on the silver clustering/aggregation is followed by a suite of *in situ* and *ex situ* physicochemical characterization techniques. The results reported here prove that besides the activation treatment and the catalysts' chemical composition, the framework topology plays a key role in the formation of silver species and thus in determining their redox properties and catalytic performance in the NH_3-SCO reaction.

2. Materials and methods

2.1 Preparation of Ag-zeolites

AgCHA(2), AgCHA(4) and AgRHO(4) zeolites were obtained by silver exchange of KCHA(2.2), KCHA(4.2) and NaCsRHO(4.4), respectively, where the values in parentheses indicate the Si/Al molar ratio. The parent zeolites were synthesized following the procedure described in the ESI† (zeolite synthesis and preliminary characterization; for XRD and FESEM images, see Fig. S1 and S2†). The Ag^+ exchange was carried out using an aqueous solution of $AgNO_3$ (ACS reagent 99.9%) in the appropriate concentration in order to obtain Ag/Al = 1 using a solid/liquid ratio of 1/100 at 25 °C for 16 h, under mechanical stirring and in darkness to avoid reduction of Ag^+ to Ag^0. Then, the solids were filtered in darkness, washed with distilled water to remove excess silver, dried at 100 °C for 24 h and stored in darkness. The chemical composition of the Ag-zeolites is shown in Table 1. The Na^+ ions present in the parent NaCsRHO(4) zeolite are selectively replaced by silver, most likely due to its smaller ionic diameter, while Cs^+ remains in AgRHO(4). The XRD patterns of the AgCHA(2), AgCHA(4) and AgRHO(4) samples are similar to those of the as-synthesized silver-free zeolites (see Fig. S3†). A AgNaRHO(4) zeolite with a chemical composition similar to that of AgRHO(4) (see Table 1) was prepared by subsequent Na^+ exchange until Cs^+ was fully replaced. Then, Ag^+ exchange was performed as previously described.

Ag-zeolite samples were thermally reduced under a diluted H_2 flow (100 mL min^{-1}, 10% H_2/He) at 400 °C for 40 min at a heating rate of 10 °C min^{-1} and labeled as AgCHA(2)-R, AgCHA(4)-R and AgRHO(4)-R. Then, the reduced zeolites were treated in a diluted O_2 flow (100 mL min^{-1}, 10% O_2/He) at 400 °C for 40 min at a heating rate of 10 °C min^{-1} and named AgCHA(2)-R-Ox, AgCHA(4)-R-Ox and AgRHO(4)-R-Ox.

2.2 Characterization techniques

X-ray diffraction (XRD) patterns were recorded using a Panalytical CubiX3 diffractometer operating at 45 kV and 40 mA and using Cu Kα radiation. The experimental XRD patterns of the Ag-zeolites were compared to those of Ag^0 (00-004-0783) and Ag_2O (00-012-0793) JCPDS crystallographic files.

FESEM images were taken using a ZEISS Ultra-55 microscope. The sample powder was deposited using double-carbon-sided tape and analyzed without metal covering.

^{109}Ag solid-state NMR spectra were recorded at room temperature with a Bruker AV III HD 400 spectrometer at 18.60 MHz using a 7 mm probe spinning the samples at 5 kHz, 14 μs as a 90° pulse and 3 s as a recycle delay. Ag_3PO_4 was used as a secondary reference (δ ^{109}Ag = 342.5 ppm).[34]

A UV-Vis Cary 5000 spectrometer equipped with a diffuse reflectance accessory (Praying Mantis Harrick) was used for recording UV-Vis spectra and $BaSO_4$ was used as a standard for background measurement. The spectra of Ag-zeolites after reduction were immediately measured after H_2 treatment to avoid silver oxidation.

FT-IR experiments were performed using a Vertex 70 spectrometer (Bruker). Before FT-IR studies, the zeolite samples

Table 1 Chemical composition of Ag-loaded zeolites

Sample	Si/Al_{EDX}	Si/Al_{NMR}	Ag/Al_{EDX}	$(Ag^+ + M^+)/Al_{EDX}$	Ag wt%
AgCHA(2)	2.2	2.2	0.7	1.0 (K^+)[a]	26
AgCHA(4)	4.2	4.1	0.5	0.9 (K^+)[a]	14
AgRHO(4)	4.4	4.5	0.7	1.1 (Cs^+)[a]	16
AgNaRHO(4)	4.3	—	0.6	0.9 (Na^+)[a]	16

[a] Co-cation (M^+ = Cs^+, K^+, Na^+) present after the silver ion-exchange procedure. Similar Si/Al ratios were obtained by EDX and ^{29}Si NMR, excluding extra framework Al, as confirmed by ^{27}Al NMR spectroscopy.

were pressed into self-supporting wafers (*ca.* 5 mg cm^{-2}) and thermally treated in an *in situ* IR cell at 400 °C at a heating rate of 10 °C min^{-1} under vacuum for 30 min. Then, the samples were cooled down to 200 °C, and reduced with deuterium (106 mbar, MATHESON) at this temperature up to 300 s. Subsequently, the samples were evacuated at 200 °C for 20 min and oxidized with O_2 (106 mbar, MESSER, 5.0) at the same temperature up to 300 s. Rapid scan FT-IR spectra were recorded every 0.6 s under *operando* conditions during the reduction and subsequent oxidation at 200 °C. This temperature was chosen as most suitable for following the reversibility of the reduction–oxidation process to ensure the removal of formed water. Afterward, the samples were heated up to 400 °C at 10 °C min^{-1} and kept for 20 min in contact with O_2. After the oxidation process, the samples were cooled down to room temperature and *in situ* CO sorption (PRAXAIR, 4.8) was performed. Based on earlier studies,[19,35] quantitative analysis of the Ag species present in the samples was carried out.

X-ray absorption experiments at the Ag K-edge (25 514 eV) were performed at the BL22 (CLÆSS) beamline of the ALBA synchrotron (Cerdanyola del Vallès, Spain).[36] The white beam was monochromatized using a Si (311) double crystal cooled by liquid nitrogen; harmonic rejection has been performed using Rh-coated silicon mirrors. The spectra were collected in transmission mode by means of ionization chambers filled with appropriate gases (88% N_2 + 12% Kr for I_0 and 100% Kr for I_1). Samples in the form of self-supported pellets of optimized thickness have been located inside an *in situ* cell described by Guilera *el al.*[37] XAS spectra of the samples were collected upon reduction at 100 °C, 200 °C and 400 °C following the temperature profiles shown in Fig. S4.† All the samples were subsequently oxidized at 400 °C following the profile shown in Fig. S4a.† Several scans were acquired at each measurement step (allowing 20 min for temperature stabilization in each step) to ensure spectral reproducibility and a good signal-to-noise ratio. The data reduction and extraction of the $\chi(k)$ function have been performed using the Athena code.[38] EXAFS data analysis has been performed using Artemis software.[38] The methodology of data fitting consists of a co-refinement approach in which determined parameters are constrained to decrease correlation problems usually found in XAS data analysis. As a common strategy, ΔE_0 is allowed to vary but is fixed (and equal) for spectra with atoms in the same local environment and the Debye–Waller factor (DWF) can be constrained considering similar disorder within the absorber atoms. This strategy was adopted due to the reliability of the fits in terms of small errors. Additional information will be displayed as a note below the table of EXAFS results. Phases and amplitudes have been calculated with the FEFF6 code using crystallographic files for well-known Ag-based standards as input. In the case of the as-obtained AgCHA(2) and AgRHO(4) spectra, crystallographic data of similar materials were used, which were modified to obtain experimentally reasonable results.

2.3 NH_3-SCO catalytic experiments

NH_3-SCO-activity measurements over the Ag-zeolite catalysts were carried out in a fixed-bed quartz tubular reactor of 1.2 cm diameter and 20 cm length, using a gas mixture of 500 ppm NH_3, 7 vol% O_2 and N_2 as a balance. The total flow rate and amount of catalyst were 0.8 L min^{-1} and 0.25 g, respectively, resulting in a 192 L h^{-1} g^{-1} WHSV for the catalytic experiments. Three online detectors were used to analyze the outlet gases: a UV-based detector for monitoring NH_3 (Tethys Instruments EMX400), an infrared analyzer for N_2O analysis (Servomex 4900) and a chemiluminescence analyzer which allows the quantification of NO_x concentration (Thermo 42C).

3. Results and discussion

The silver-exchanged zeolites with the chemical compositions summarized in Table 1 were characterized by the combination of several spectroscopic techniques. All samples have similar Ag/Al molar ratios ≈ 1, suggesting that all Ag-zeolites underwent nearly full Ag^+ exchange. Thus, AgCHA(2) with a lower Si/Al ratio (Si/Al ≈ 2) has higher silver content (∼26 wt%) than the two other AgCHA(4) and AgRHO(4) zeolites (Si/Al ≈ 4; ∼15 wt% Ag). The presence of compensating Ag^+ cations was confirmed by EXAFS data (Fig. S5, S6 and Table S1†), which show that Ag^+ is coordinated to two O atoms at Ag–O distances of 2.26 Å and 2.43 Å, respectively, with an average coordination number close to three, in good agreement with previous results reported for the AgLTA zeolite.[39] The presence of silver as Ag^+ in the Ag-zeolites is further supported by a signal at δ ^{109}Ag around 40 ppm in the solid-state NMR spectra and a band at 220 nm in the UV-Vis spectra (see Fig. S7†).

3.1 The state of silver in Ag-zeolites upon reduction under hydrogen

The reduction of Ag^+ was studied by treating the Ag-exchanged zeolites under hydrogen at 400 °C. The X-ray diffractograms, displayed in Fig. 1, show the characteristic patterns of the CHA- (Fig. 1a) or RHO- (Fig. 1b) type zeolite accompanied by the characteristic diffraction lines of silver metal, with a relative intensity that depends on the sample. So, the diffraction peaks of the Ag^0 metal are considerably less intense for the AgRHO(4)-R when compared with the AgCHA(4)-R with similar silver loading, indicating that at least in sample AgRHO(4)-R, there must be smaller NPs or other species such as metal clusters, not observable by XRD. To gain additional information on the species formed, the reduced Ag-zeolite samples were characterized by XAS and UV-Vis spectroscopies.

Fig. 2 shows the |FT| spectra of the AgCHA(2)-R, AgCHA(4)-R and AgRHO(4)-R zeolites and of silver foil used as a reference, all of them containing only a peak centered at about 2.6 Å due to the Ag–Ag bond. The intensity of the Ag–Ag peak for the two AgCHA zeolites is similar to that of metal foil, while that of AgRHO(4)-R is considerably weaker. Indeed, the analysis of the EXAFS oscillations (curve-fittings shown in Fig. S8†) leads to the structural data summarized in Table 2. The Ag–Ag coordination number is similar to that of the metal foil (CN_{Ag-Ag} ≈ 12) for the two chabazite samples (AgCHA(2)-R and AgCHA(4)-R) and significantly smaller (CN_{Ag-Ag} ≈ 8.6) for the AgRHO(4)-R zeolite. Therefore, besides silver NPs, the AgRHO(4)-R zeolite must

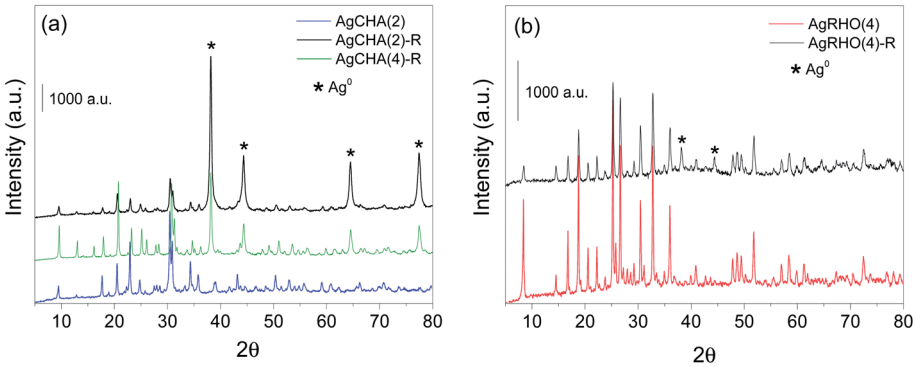

Fig. 1 X-ray diffractograms of AgCHA (a) and AgRHO (b) zeolites in their as-obtained and reduced states.

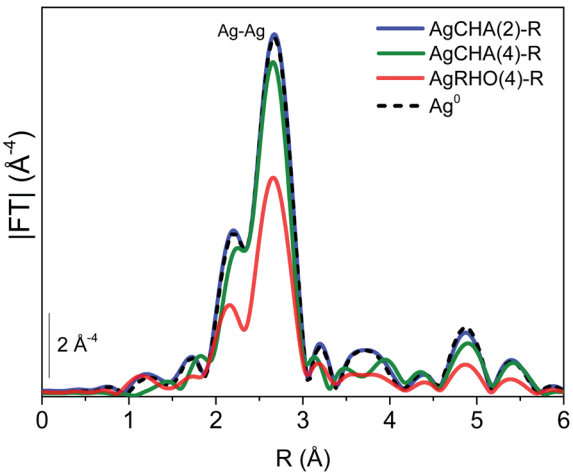

Fig. 2 |FT| of the k^3-weighted EXAFS spectra of the AgCHA(2), AgCHA(4) and AgRHO(4) zeolites treated under hydrogen at 400 °C. The reduced samples were cooled down to RT under a H_2 atmosphere before data collection to minimize the DWF and allow direct comparison.

contain small aggregates of silver atoms, thus decreasing the average Ag–Ag coordination number.

The complete reduction of isolated Ag^+ cations is supported by the absence of any signal in the high field spectral region of the ^{109}Ag NMR (δ ^{109}Ag $\approx$ 40 ppm) representative of Ag^+ (Fig. S9†). Indeed, the spectra of the reduced Ag-zeolites consist of a unique resonance at δ ^{109}Ag $\approx$ 5270 ppm assigned to Ag^0 as illustrated in Fig. 3 for the AgCHA(2)-R and AgRHO(4)-R zeolites. The shape of the peak of AgCHA(2)-R is quite similar to that of silver metal used as a reference, while that of AgRHO(4)-R is significantly narrower in agreement with the lower aggregation of silver in this sample.

The differences in the aggregation state of silver in the AgCHA and AgRHO samples are evidenced by the UV-Vis spectra shown in Fig. 4. The two AgCHA zeolites yield similar spectra displaying two broad bands with one maximum at 375–400 nm assigned to silver NPs and another one at ~275 nm that may contain signals from $Ag_m^{\delta+}$ and/or Ag_n^0 clusters.[40] Meanwhile, the spectrum of the AgRHO(4)-R zeolite (see Fig. 4) is quite different, presenting distinct absorption bands in the region between 250 nm and 400 nm. Although the interpretation of the UV-Vis spectra and the assignment of the UV-Vis bands to specific silver species are uncertain, according to literature data, the bands at 310 nm and 325 nm can be tentatively assigned to Ag_8 and the band at $\approx$360 nm to larger Ag_n^0 clusters. It must be noted that the spectrum of the AgRHO(4)-R zeolite also shows a weak component at 400–450 nm indicating the presence of some metal NPs.[40] Fig. S10† shows the TEM images of the AgCHA(2)-R and AgRHO(4)-R zeolites (reduced under H_2 at 400 °C). In this figure, it is evident that AgRHO(4)-R zeolite has

Table 2 Summary of the EXAFS fit of the reduced Ag-loaded zeolites[a]

Sample	CN	R (Å)	σ^2 (Å^2)	ΔE_0 (eV)	r-factor
AgCHA(2)-R	11.1(8)	2.852(12)	0.0093(6)	2.0(5)	0.0045
AgCHA(4)-R	11.3(6)	2.857(2)	0.0102(5)		0.0029
AgRHO(4)-R	8.6(7)	2.850(14)	0.0114(9)		0.0085
AgNaRHO-R	9.3(5)	2.845(3)	0.0124(6)		0.0032

[a] The fits were performed on the first coordination shell (ΔR = 2.0–3.0 Å) over FT of the $k^1k^2k^3$-weighted $\chi(k)$ functions performed in the Δk = 2.3–11.8 Å^{-1} interval. S_0^2 = 0.80.

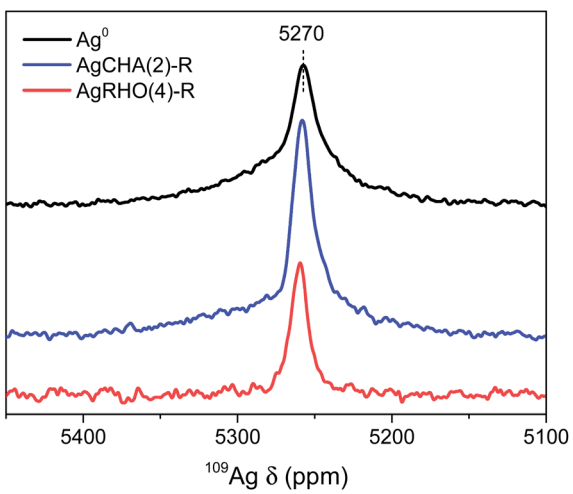

Fig. 3 ^{109}Ag MAS NMR spectra of Ag metal and AgCHA(2) and AgRHO(4) zeolites treated under hydrogen at 400 °C.

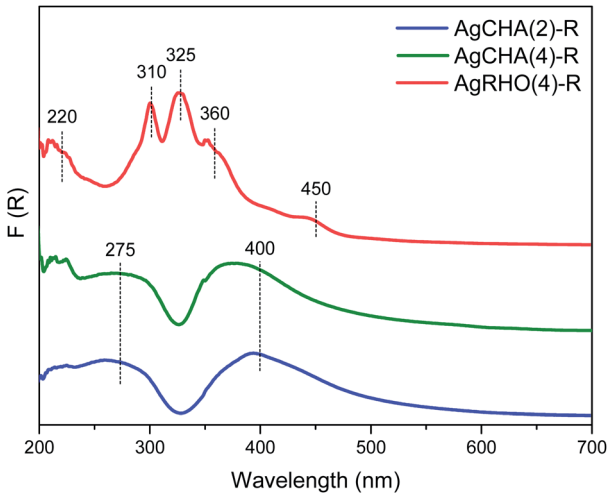

Fig. 4 UV-Vis spectra of AgCHA(2), AgCHA(4) and AgRHO(4) treated under H_2 at 400 °C.

a much lower concentration of metal nanoparticles at its external surface. This indirectly indicates that most of the Ag remains inside the zeolite cavities as clusters.

Therefore, the results reported here indicate that although some metal NPs must be present, silver clusters are dominant in the AgRHO(4)-R zeolite, while most silver atoms are involved in metal NPs in the two Ag-chabazites. Besides the zeolite topology, the main difference between the two types of material is the alkaline co-cation compensating for the framework charge, K^+ for the two AgCHA zeolites and Cs^+ for the AgRHO zeolite. The Cs^+ acting as a compensating co-cation in the AgRHO(4) zeolite is bulkier than the K^+ and might hinder the diffusion of silver atoms within the zeolite, inhibiting the formation of metal NPs at relatively high temperatures. To check this hypothesis, the AgNaRHO zeolite with a chemical composition similar to AgRHO(4) but containing Na^+ instead of Cs^+ (see Table 1) was prepared and the corresponding reduced sample (at 400 °C) was analyzed by XAS and UV-Vis spectroscopies (Fig. S11 and S12).† The curve-fitting of the EXAFS oscillations of the AgNaRHO zeolite (Fig. S11†) gives a Ag–Ag coordination number of ~9.3 and $R_{Ag-Ag} \approx 2.84$ Å, close to those obtained for AgRHO(4)-R (see Table 2), indicating that the average Ag–Ag coordination is similar for the two AgRHO zeolites containing Cs^+ or Na^+ as a co-cation. Also, the UV-Vis spectra of AgNaRHO(4)-R and AgRHO(4)-R (see Fig. S12†) are consistent with the predominance of silver clusters in the two samples. These results confirm that the preferred formation of small aggregates of few silver atoms in the AgRHO zeolite and of Ag^0 NPs in the AgCHA zeolites is determined by the framework topology and not by the alkaline co-cation.

Since Ag NPs are the predominant Ag species in AgCHA zeolites upon reduction at 400 °C, the study of Ag aggregation under reduction conditions was performed at lower temperatures. The analysis of the EXAFS data and the UV-Vis spectra of the AgCHA(2) reduced at 100 °C and 200 °C are provided in the ESI (Fig. S13–S15†). The |FT| of the EXAFS data shows the growth of the Ag–Ag peak as the temperature rises from 100 °C to 200 °C, but with the intensity lower than that of the silver foil. Indeed the Ag–Ag coordination number of AgCHA(2) is around $N_{Ag-Ag} \approx 7$ at 200 °C (Table S2†). Accordingly, the UV-Vis spectra (Fig. S15†) show discrete absorption bands between 250 nm and 400 nm, indicating that silver clusters are the main species in the AgCHA(2) zeolite reduced at 100–200 °C. Therefore, it is possible to stabilize silver clusters of few atoms in the AgCHA zeolite by decreasing the reduction temperature. Comparing this behavior to that observed for the AgRHO(4) zeolite, it can be concluded that similar Ag species are formed in both materials but at different temperatures, suggesting that the reducibility of Ag species differs depending on the zeolite structure.

Thus, the influence of the framework topology on the reducibility of atomic Ag^+ at 200 °C to form silver clusters was investigated by means of rapid scan FT-IR spectroscopy (one spectrum taken every 0.6 s) under *operando* conditions using D_2. To keep the charge neutrality of the Ag-zeolites, the reduction of Ag^+ to Ag^0 is accompanied by the formation of Si(OD)Al groups, which gives high frequency (HF) $Si(OD)Al_{HF}$ and low frequency

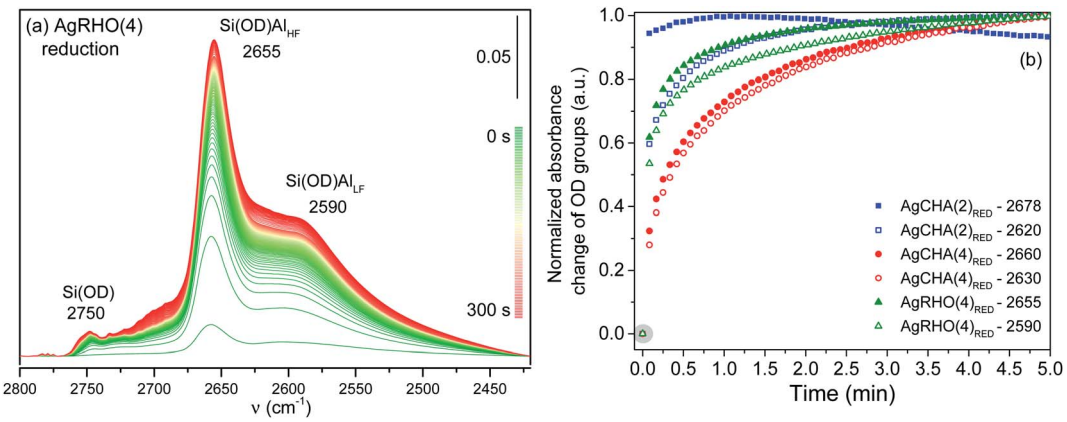

Fig. 5 (a) Time-resolved rapid scan FT-IR spectra in the region of O–D stretching vibrations of AgRHO(4) in contact with D_2 at 200 °C for 5 min. (b) Normalized trace of the absorbance change of high- and low-frequency OD group bands during reduction with D_2 at 200 °C for 5 min. Note: the grey circle represents the starting point (in time) of all normalized bands.

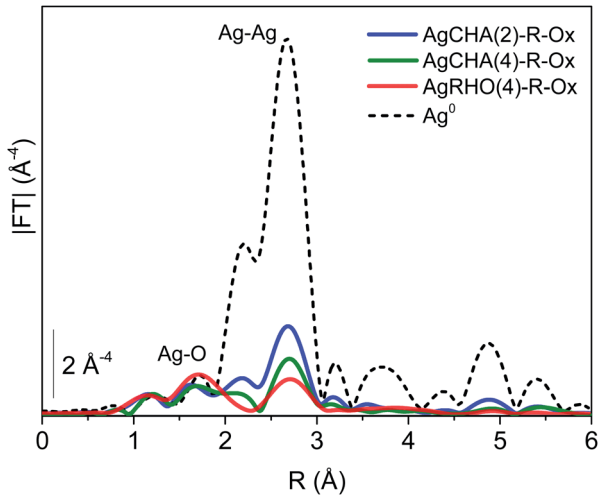

Fig. 6 |FT| of the k^3-weighted EXAFS spectra of the AgCHA(2), AgCHA(4) and AgRHO(4) samples reduced at 400 °C and subsequently treated under O_2 at 400 °C.

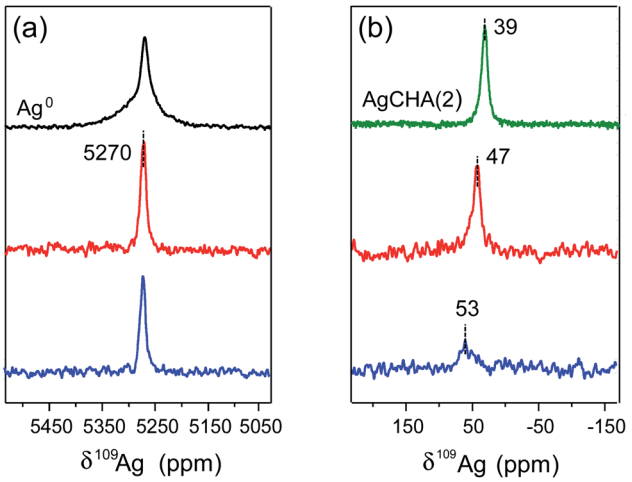

Fig. 7 ^{109}Ag MAS NMR spectra in the regions of Ag^0 (a) and Ag^+ (b) of the AgCHA(2)-R-Ox (blue) and AgRHO(4)-R-Ox (red) zeolites. Ag metal (black) and AgCHA(2) (green) are the references for Ag^0 and Ag^+, respectively.

(LF) Si(OD)Al_{LF} bands in the 2800–2450 cm^{-1} region associated with different oxygen sites of the zeolite framework. The development of OD bands as a function of the heating time is illustrated in Fig. 5a for zeolite AgRHO(4) (Fig. S16† for zeolites AgCHA(2) and AgCHA(4)) while Fig. 5b compares the evolution of the normalized intensity of the HF and LF bands for the three Ag-zeolites. For the CHA type structure, the HF band is associated with –OD groups exposed to the barrel-shaped cages (*rth* cavity), which are interconnected by eight-membered ring windows.[41] The data plotted in Fig. 5b indicate that the HF band appears immediately after adding D_2 for the AgCHA(2) sample and reaches the maximum intensity after heating for 50 s, whereas it requires at least 150 s for AgCHA(4), indicating that the aggregation of Ag_n^0 in the CHA cavities is favoured at higher silver loading. Regarding the kinetics of Ag reduction, the intensity of the Si(OD)Al bands increases more rapidly for the AgRHO(4) than for the AgCHA(4) zeolite. Thus, when the two zeolite types having similar Si/Al molar ratio are considered, the reduction is more favorable for AgRHO than for AgCHA zeolites.

3.2 The state of silver after oxidation of reduced Ag-zeolites

As mentioned in the introduction, heating under an oxidizing atmosphere increases the dispersion of noble metal particles and may be a potential alternative for obtaining silver clusters or even atomically dispersed species in small pore zeolites. For this purpose, the AgCHA and AgRHO zeolites reduced at 400 °C, containing mainly NPs and clusters, respectively, were treated under oxygen at 400 °C and fully characterized to identify the formed silver species.

The XRD patterns of the Ag-zeolites show that oxidation of the reduced zeolites provokes a sharp decrease in the intensity of the peaks of metallic Ag in the AgCHA zeolites and their disappearance in the AgRHO (see Fig. S17†). These changes indicate that, effectively, the oxidation treatment provokes the dispersion of the silver NPs in the two zeolites. More information is gained by the study of the oxidation process by means of XAS and UV-Vis spectroscopies.

Fig. 6 shows the |FT| of the k^3-weighted EXAFS spectra of the Ag-zeolites reduced and oxidized at 400 °C (AgCHA(2)-R-Ox, AgCHA(4)-R-Ox, and AgRHO(2)-R-Ox). Comparison of the spectra of the reduced samples (see Fig. 2) with those of the oxidized materials (Fig. 6) shows a sharp decrease of the Ag–Ag contribution indicating the dispersion of the metal NPs. Moreover, the spectra show a peak of Ag–O similar to that observed in the as-prepared samples suggesting that some silver is oxidized to Ag^+, besides the metal dispersion. The shapes of the FT spectra of the two AgCHA samples are similar, while that of the AgRHO(2)-R-Ox zeolite is slightly different, with a smaller Ag–Ag contribution and larger Ag–O signal than those observed in CHA zeolites. Quantitative estimation of the Ag–Ag coordination number and interatomic distances is challenging due to overlapping between the contributions from the scattering of silver nanoparticles and the higher shells of cationic silver. Nevertheless, the main features of the FT spectra of the oxidized Ag-zeolites indicate that Ag^0 NPs are dispersed and oxidized to Ag^+ upon treatment under O_2 to a higher extent for the AgRHO zeolite.

Further information on the oxidation state of the dispersed species on the oxidized samples was obtained by solid-state NMR and UV-Vis spectroscopies. The ^{109}Ag NMR spectra of the AgCHA(2)-R-Ox and AgRHO(4)-R-Ox zeolites, shown in Fig. 7, contain two peaks at δ ^{109}Ag $\approx$ 5270 ppm (Fig. 7a) and δ ^{109}Ag $\approx$ 40–50 ppm (Fig. 7b) assigned to Ag^0 and Ag^+, respectively. The relative intensity of the peak of Ag^+ and the extent of silver oxidation is greater for the AgRHO(4) than for the AgCHA(2). It is interesting to note that the peak of Ag^0 of the AgCHA(2)-R-Ox sample becomes narrower than that of the reduced sample, suggesting smaller NPs.

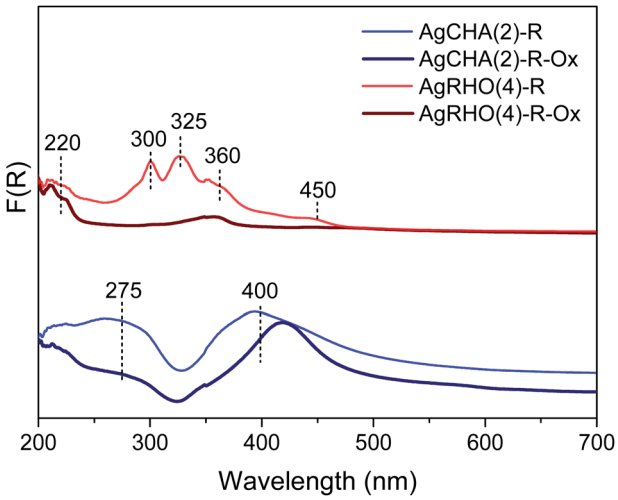

Fig. 8 UV-Vis spectra of AgCHA(2) and AgRHO(4) zeolites treated under hydrogen at 400 °C and then under O_2 at 400 °C.

Fig. 8 compares the UV-Vis spectra of the AgCHA(2) and AgRHO(4) zeolites reduced and oxidized at 400 °C. The spectrum of the AgCHA(2)-R sample after oxidation shows an intensity decrease in the region around 275 nm, which suggest that silver clusters are oxidized to Ag^+, being supported by the appearance of a new band at 220 nm.[40] Meanwhile, the UV-Vis spectrum of the AgRHO(4)-R zeolite suffers important changes after oxidation. The disappearance of the bands at 300 and 325 nm indicates that Ag clusters evolve mostly to Ag^+, as suggested by the evolution of the band at 220 nm. Meanwhile, the weak signal at 360 nm, attributed to Ag_n^0 clusters or small NPs,[40] remains. Therefore, the whole set of physicochemical characterization spectroscopies clearly indicates that the oxidation of the reduced Ag-zeolites causes the dispersion of silver NPs and the formation of cationic Ag^+, to a higher extent on the AgRHO zeolite because it contains silver clusters. This is further supported by studying AgCHA samples pre-reduced at 100 °C and 200 °C that contain mostly silver clusters. These samples upon oxidation yield mostly cationic Ag^+ (see Fig. S18–S19†).

Table 3 The concentration of Ag^+ and Ag^0 species in Ag-loaded zeolites determined from FT-IR quantitative experiments of CO sorption at RT and the total concentration of Ag derived from chemical analysis

Sample	Ag/u.c. EDX	Ag^+ (FT-IR)	Ag^0 (FT-IR)	$Ag^+ + Ag^0$ (FT-IR)
$AgCHA(2)_{R2O}$[a]	7.4	3.9	0.2	4.1
$AgCHA(4)_{R2O}$[a]	3.7	3.6	0.1	3.7
$AgRHO(4)_{R2O}$[a]	6.0	5.9	0.0	5.9

[a] The nomenclature R2O after the Ag-zeolite name stands for reduced at 200 °C and subsequently oxidized under O_2.

The whole evolution of Ag^+ has been completed by studying the oxidation at 200 °C of the Ag-zeolites pre-reduced at this same temperature according to the experiment depicted in Fig. 5 for the AgRHO(2) zeolite (Fig. S16† for the AgCHA samples). The FT-IR spectra recorded under *operando* conditions during oxidation are presented in Fig. 9a for the AgRHO(4) zeolite (and in Fig. S20† for the AgCHA samples). The Ag^+ formed upon oxidation compensates for the negative framework charges, thus decreasing the number of Si(OD)Al groups, which can be monitored by the intensity decrease of the corresponding FT-IR bands. The results, plotted in Fig. 9b, show that the oxidation of silver to Ag^+ at 200 °C is almost complete after 3 min in the two AgCHA samples, whereas it reaches completion after 20 min for the AgRHO(2) zeolite (only about 20% is oxidized in 5 min).

The relative stability of the silver clusters at a higher temperature was studied by oxidizing at 400 °C for 20 min the samples pre-reduced with D_2 at 200 °C. The quantitative analysis of Ag^+ and Ag^0 species was carried out by means of infrared spectroscopy using CO as a probe molecule and the absorption coefficients of the Ag^+(CO) and Ag^0(CO) bands. The results, summarized in Table 3, show that the amount of Ag^+ plus Ag^0 in AgCHA(2) (reduced at 200 °C and oxidized at 400 °C) is considerably lower than the metal loading, indicating that silver

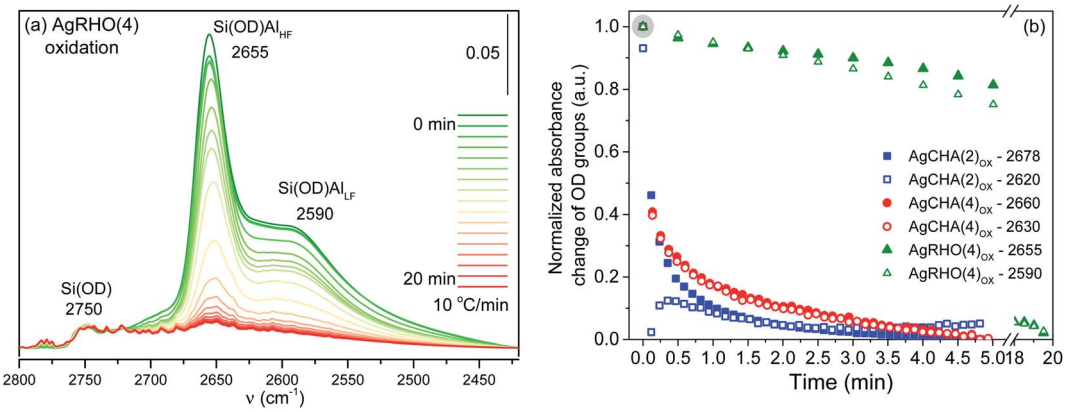

Fig. 9 (a) Time-resolved rapid scan FT-IR spectra in the region of O–D stretching vibrations of the AgRHO zeolite in contact with O_2 for 20 min during heating up to 400 °C. (b) Normalized trace of the absorbance change of high- and low-frequency OD group bands during oxidation with O_2 at 200 °C.

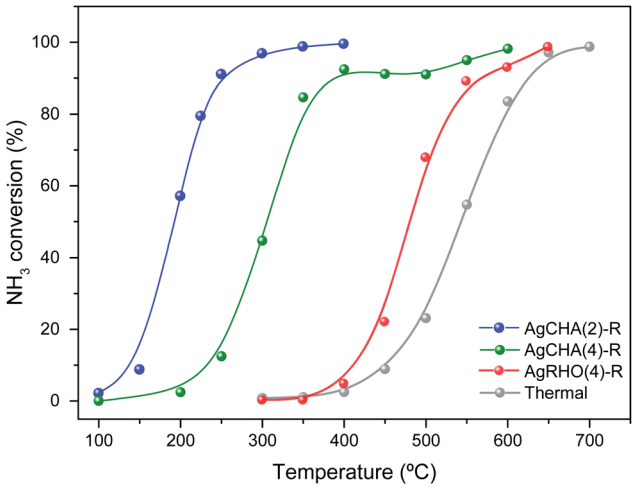

Fig. 10 Catalytic activity in the NH_3-SCO reaction of AgCHA(2), AgCHA(4) and AgRHO(4) reduced at 400 °C.

clusters and/or NPs persist after oxidation. Meanwhile, practically all silver is in the form of Ag^+ in the AgCHA(4) and AgRHO(4) samples with lower metal loadings (Table 3). Therefore, silver is completely oxidized in Ag-zeolites with lower Ag content at 400 °C, in good agreement with the UV-Vis results.

3.3 Ag-zeolites as catalysts for the NH_3-SCO reaction

Fig. 10 shows the light-off curves for the NH_3 conversion during the NH_3-SCO reaction on the AgCHA(2)-R, AgCHA(4)-R and AgRHO(4)-R zeolites, as well as the blank reaction run without any catalyst. There, it can be seen that the most active catalyst is AgCHA(2)-R ($T_{50\%}$ = 200 °C) followed by AgCHA(4)-R ($T_{50\%} \approx$ 275 °C) and the less active AgRHO(4)-R ($T_{50\%}$ = 475 °C), while the $T_{50\%}$ for the thermal test is 550 °C. Thus, for the same zeolite structure (CHA type), in which the metal forms NPs, the activity increases with the silver loading. However, the AgRHO(4)-R zeolite is less active than AgCHA(4)-R despite the fact that they have similar chemical composition. This can be associated with the presence of silver clusters (*i.e.* absence of Ag NPs) in the AgRHO catalyst or with the blockage of the porosity by Ag species placed at the external surface of the RHO zeolite. We have excluded the latter possibility based on (i) the CO_2 adsorption at 0 °C (see Fig. S21†) following the IUPAC recommendation for ultra-microporous solids[42] that unambiguously confirms the microporous nature of the AgRHO adsorbing 4.5 mmol CO_2 per g (see Fig. S21†) and (ii) the ammonia adsorption followed by a thermo-programmed desorption experiment coupled with mass spectrometry (TPD-MS) and adsorption and stepwise desorption of ammonia followed by IR spectroscopy (see Fig. S22 and S23† and the accompanying discussion in the ESI†). Thus, it may be concluded that Ag clusters are nearly inactive for the selective oxidation of ammonia.

The NH_3 conversion in the NH_3-SCO reaction at 400 °C of the AgCHA(2)-R is 100% and the sample keeps its brown coloration after the test. Meanwhile, the conversion is practically null for the AgRHO(4) zeolite at this temperature and its color turns white after the reaction. To gain further insight into the silver species, UV-Vis spectra of the post-mortem AgCHA(2) and AgRHO(4) zeolites were measured after the catalytic test at 400 °C and are compared with those of the samples reduced at 400 °C in Fig. 11. The spectrum of the AgCHA(2)-R sample after reaction shows a decrease in the intensity of the band at ≈275 nm, assigned to silver clusters and the growth of the intensity of the band at 220 nm attributed to Ag^+, while the band at 420 nm of NPs remains. The UV-Vis spectrum of the post-mortem AgRHO(4)-R zeolite also changes, being mainly formed by the signals at 220 nm and 355 nm assigned to Ag^+ and to Ag_n^0 clusters, respectively. These results are supported by an *in situ* EXAFS. The |FT| spectra of the zeolites treated under reaction conditions at 550 °C and measured at room temperature indicate that while the NPs still exist in the used AgCHA(2)-R sample, total oxidation to Ag^+ occurs in the AgRHO(4)-R catalyst (see Fig. S24†). Finally, XRD data of the post-mortem catalysts further support the UV-Vis and XAS results. Indeed, Ag^0 peaks are clearly visible in the patterns of the reduced samples (see Fig. S25†). After NH_3-SCO reaction, the metallic Ag XRD reflections disappear or strongly diminish, while the characteristic peaks of the zeolite at low angle decrease their intensities. These findings suggest that Ag^0 species are oxidized to Ag^+ during the NH_3-SCO reaction and these cationic Ag^+ species compensate for the negative charge of the zeolite framework in the recovered catalysts after the reaction.

Therefore, silver NPs are much more active for the NH_3-SCO reaction than silver clusters, which are practically non-active below 400 °C.

3.4 General remarks

The results presented here give an overview on the silver species formed in the AgCHA and AgRHO zeolites submitted to different treatments. In the as-prepared materials, the Ag^+ and alkaline

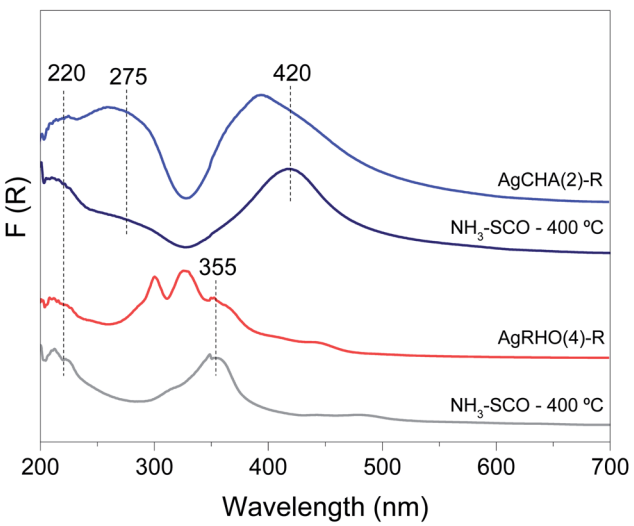

Fig. 11 UV-Vis spectra of (top) the AgCHA(2) zeolite reduced at 400 °C and after the NH_3-SCO reaction at 400 °C, and (bottom) the AgRHO(4) zeolite reduced at 400 °C and after the NH_3-SCO reaction at 400 °C.

cations are placed at exchange positions compensating for the negative charges associated with the presence of framework aluminum. Heating the Ag-zeolites under hydrogen provokes the reduction of Ag^+ to form silver clusters within the small cages and/or NPs placed at the external surface of the zeolite. The reduction process is accompanied by the formation of Brønsted acid sites needed to keep the charge neutrality of the material. Meanwhile, the opposite effect occurs upon the oxidation of pre-reduced Ag-zeolites, *i.e.*, the redispersion and oxidation of clusters or NPs and even formation of Ag^+ with the concomitant decrease in the number of Brønsted acid sites. Thus, different proportions of isolated Ag^+, neutral or positively charged clusters and metal NPs are present in the Ag-zeolites depending on the specific reduction–oxidation treatment and most remarkably on the framework topology.

The results presented here show that the silver species present in the small pore RHO- and CHA-type zeolites submitted to the same treatment are different, indicating that there exists a strong dependence on the structure. Silver clusters of few atoms are the main species in both AgCHA and AgRHO zeolites after reduction at low temperature (at 100 °C and 200 °C). However, when the temperature is raised to 400 °C no significant changes occur in AgRHO, while silver clusters aggregate to form NPs in the AgCHA zeolite. The results obtained after subsequent treatment under O_2 at 400 °C indicate that the degree of silver oxidation depends on the initial state in the pre-reduced Ag-zeolites. Thus, the aggregates of few atoms are fully oxidized to atomic Ag^+, while metal NPs are more resistant against oxidation, being only partially dispersed and then oxidized to Ag^+. Indeed, the results obtained by FT-IR spectroscopy under *operando* conditions on the reduction–oxidation of Ag-zeolites at 200 °C show that silver clusters are easier to form and more resistant to oxidation in the RHO-type than in the CHA-type structure. Thus, silver clusters are stabilized in the RHO-type structure persisting after the treatment under H_2 at 400 °C, while they aggregate in the chabazite, proving that the zeolite topology strongly affects the nature of formed silver species.

The stabilization of sub-nanometer silver agglomerates within the zeolite cavities has important consequences on the physico-chemical properties of Ag-zeolites, but also on their catalytic application, as illustrated here for the NH_3-SCO reaction. The AgCHA zeolites reduced at 400 °C are very active for the NH_3-SCO reaction, as they contain metal NPs which are the most probable active sites. However, the AgRHO zeolite reduced at 400 °C in which the metal forms clusters is practically inactive for this reaction. Although it is not well established yet, this result proves that silver sub-nanometric aggregates are inactive for the NH_3-SCO reaction. Moreover, silver clusters and metal NPs also display different stabilities under the reaction conditions since silver clusters are completely oxidized to Ag^+ at 400 °C, which is also inactive for the reaction, while metal NPs persist.

These results prove that the choice of the zeolite topology is of key importance to develop Ag-zeolites optimized for a particular application in catalysis or any other field.

4. Conclusions

The results reported here indicate that the concentration and stability of silver species, *i.e.*, Ag^+, silver clusters and metal NPs formed in AgCHA and AgRHO zeolites, depend on the specific reduction/oxidation conditions and more importantly on the zeolite topology. Reduction at 100–200 °C gives rise to the formation of silver clusters in the two zeolites. When the temperature is raised to 400 °C, NPs are developed in the CHA-type while small aggregates persist in the RHO-type zeolite, indicating that they are highly stable in this structure. Silver NPs formed in the AgCHA zeolite reduced at high temperature are active for the NH_3-SCO reaction, while silver clusters present in the AgRHO zeolite even reduced at 400 °C are inactive for the reaction. These species also display different stabilities under oxidative conditions, so that metal NPs persist while silver clusters are completely oxidized to Ag^+ under oxidizing conditions or reaction conditions at 400 °C.

Conflicts of interest

There are no conflicts to declare.

Acknowledgements

The authors acknowledge grant RTI2018-101784-B-I00 funded by MCIN/AEI/10.13039/501100011033 and by "ERDF A way of making Europe". Also, the project SEV-2016-0683 funded by MCIN/AEI/10.13039/501100011033 is acknowledged. The project Prometeo/2021/077, Conselleria de Educación, Cultura y Deporte de la Generalitat Valenciana is also acknowledged. K. G.-M. acknowledges Grant No. 2015/18/E/ST4/00191 from the National Science Centre, Poland. K. T. acknowledges the scholarship within the Bekker Programme (PPN/BEK/2018/1/00406) from the Polish National Agency for Academic Exchange. C. W. Lopes (Science without Frontiers – Process no. 13191/13-6) thanks Coordenação de Aperfeiçoamento de Pessoal de Nível Superior – Brasil (CAPES – Finance Code 001) for the predoctoral fellowship. J. Martínez-Ortigosa (SEV-2012-0267-02) acknowledges the Severo Ochoa Program for a predoctoral fellowship. We gratefully acknowledge the ALBA synchrotron for allocating beamtime (proposals 2016021665 and 2017032119), CLÆSS beamline staff, and particularly Carlo Marini for their help and technical support during our experiment.

References

1 L. Liu and A. Corma, Metal Catalysts for Heterogeneous Catalysis: From Single Atoms to Nanoclusters and Nanoparticles, *Chem. Rev.*, 2018, **118**(10), 4981–5079.
2 A. Baldansuren, R.-A. Eichel and E. Roduner, Nitrogen oxide reaction with six-atom silver clusters supported on LTA zeolite, *Phys. Chem. Chem. Phys.*, 2009, **11**(31), 6664–6675.
3 T. Otto, J. M. Ramallo-López, L. J. Giovanetti, F. G. Requejo, S. I. Zones and E. Iglesia, Synthesis of stable monodisperse

AuPd, AuPt, and PdPt bimetallic clusters encapsulated within LTA-zeolites, *J. Catal.*, 2016, **342**, 125–137.

4 S. Goel, S. I. Zones and E. Iglesia, Encapsulation of metal clusters within MFI *via* interzeolite transformations and direct hydrothermal syntheses and catalytic consequences of their confinement, *J. Am. Chem. Soc.*, 2014, **136**(43), 15280–15290.

5 Z. Wu, S. Goel, M. Choi and E. Iglesia, Hydrothermal synthesis of LTA-encapsulated metal clusters and consequences for catalyst stability, reactivity, and selectivity, *J. Catal.*, 2014, **311**, 458–468.

6 L. Liu, U. Diaz, R. Arenal, G. Agostini, P. Concepcion and A. Corma, Generation of subnanometric platinum with high stability during transformation of a 2D zeolite into 3D, *Nat. Mater.*, 2017, **16**(1), 132–138.

7 L. Liu, M. Lopez-Haro, C. W. Lopes, C. Li, P. Concepcion, L. Simonelli, J. J. Calvino and A. Corma, Regioselective generation and reactivity control of subnanometric platinum clusters in zeolites for high-temperature catalysis, *Nat. Mater.*, 2019, **18**(8), 866–873.

8 L. Liu, R. Arenal, D. M. Meira and A. Corma, Generation of gold nanoclusters encapsulated in an MCM-22 zeolite for the aerobic oxidation of cyclohexane, *Chem. Commun.*, 2019, **55**(11), 1607–1610.

9 N. Salam, B. Banerjee, A. S. Roy, P. Mondal, S. Roy, A. Bhaumik and S. M. Islam, Silver nanoparticles embedded over mesoporous organic polymer as highly efficient and reusable nanocatalyst for the reduction of nitroarenes and aerobic oxidative esterification of alcohols, *Appl. Catal., A*, 2014, **477**, 184–194.

10 R. A. Molla, K. Ghosh, B. Banerjee, M. A. Iqubal, S. K. Kundu, S. M. Islam and A. Bhaumik, Silver nanoparticles embedded over porous metal organic frameworks for carbon dioxide fixation *via* carboxylation of terminal alkynes at ambient pressure, *J. Colloid Interface Sci.*, 2016, **477**, 220–229.

11 A. Baldansuren, H. Dilger, R. d.-A. Eichel, J. A. van Bokhoven and E. Roduner, Interaction and Reaction of Ethylene and Oxygen on Six-Atom Silver Clusters Supported on LTA Zeolite, *J. Phys. Chem. C*, 2009, **113**(45), 19623–19632.

12 E. Coutino-Gonzalez, W. Baekelant, D. Grandjean, M. B. J. Roeffaers, E. Fron, M. S. Aghakhani, N. Bovet, M. Van der Auweraer, P. Lievens, T. Vosch, B. Sels and J. Hofkens, Thermally activated LTA(Li)–Ag zeolites with water-responsive photoluminescence properties, *J. Mater. Chem. C*, 2015, **3**(45), 11857–11867.

13 L. Liu, D. N. Zakharov, R. Arenal, P. Concepcion, E. A. Stach and A. Corma, Evolution and stabilization of subnanometric metal species in confined space by *in situ* TEM, *Nat. Commun.*, 2018, **9**(1), 574.

14 G. Agostini, S. Usseglio, E. Groppo, M. J. Uddin, C. Prestipino, S. Bordiga, A. Zecchina, P. L. Solari and C. Lamberti, From Isolated Ag + Ions to Aggregated Ag0Nanoclusters in Silver-Exchanged Engelhard Titanosilicate (ETS-10) Molecular Sieve: Reversible Behavior, *Chem. Mater.*, 2009, **21**(7), 1343–1353.

15 K. Morgan, A. Goguet and C. Hardacre, Metal Redispersion Strategies for Recycling of Supported Metal Catalysts: A Perspective, *ACS Catal.*, 2015, **5**(6), 3430–3445.

16 M. Moliner, J. E. Gabay, C. E. Kliewer, R. T. Carr, J. Guzman, G. L. Casty, P. Serna and A. Corma, Reversible Transformation of Pt Nanoparticles into Single Atoms inside High-Silica Chabazite Zeolite, *J. Am. Chem. Soc.*, 2016, **138**(48), 15743–15750.

17 T. Baba, N. Akinaka, M. Nomura and Y. Ono, Reversible redox behaviour between silver cations and silver metal particles in hydrated Ag-Y zeolites, *J. Chem. Soc., Faraday Trans.*, 1993, **89**(3), 595–599.

18 E. Coutino-Gonzalez, W. Baekelant, J. A. Steele, C. W. Kim, M. B. J. Roeffaers and J. Hofkens, Silver Clusters in Zeolites: From Self-Assembly to Ground-Breaking Luminescent Properties, *Acc. Chem. Res.*, 2017, **50**(9), 2353–2361.

19 K. Góra-Marek, K. A. Tarach, Z. Piwowarska, M. Łaniecki and L. Chmielarz, Ag-loaded zeolites Y and USY as catalysts for selective ammonia oxidation, *Catal. Sci. Technol.*, 2016, **6**(6), 1651–1660.

20 N. Popovych, P. Kyriienko, S. Soloviev, R. Baran, Y. Millot and S. Dzwigaj, Identification of the silver state in the framework of Ag-containing zeolite by XRD, FTIR, photoluminescence, 109Ag NMR, EPR, DR UV-vis, TEM and XPS investigations, *Phys. Chem. Chem. Phys.*, 2016, **18**(42), 29458–29465.

21 O. Y. Golubeva and N. Y. Ul'yanova, Stabilization of silver nanoparticles and clusters in porous zeolite matrices with Rho, Beta, and paulingite structures, *Glass Phys. Chem.*, 2015, **41**(5), 537–544.

22 F. Gao, Y. Liu, Z. Sani, X. Tang, H. Yi, S. Zhao, Q. Yu and Y. Zhou, Advances in selective catalytic oxidation of ammonia (NH3–SCO) to dinitrogen in excess oxygen: a review on typical catalysts, catalytic performances and reaction mechanisms, *J. Environ. Chem. Eng.*, 2021, **9**(1), 104575.

23 F. Wang, J. Ma, G. He, M. Chen, C. Zhang and H. He, Nanosize Effect of Al2O3 in Ag/Al2O3 Catalyst for the Selective Catalytic Oxidation of Ammonia, *ACS Catal.*, 2018, 2670–2682.

24 F. Wang, G. He, B. Zhang, M. Chen, X. Chen, C. Zhang and H. He, Insights into the Activation Effect of H2 Pretreatment on Ag/Al2O3 Catalyst for the Selective Oxidation of Ammonia, *ACS Catal.*, 2019, **9**(2), 1437–1445.

25 Z. Wang, S. Li, C. Zhang, D. Wang and X. Li, *The Opportunities and Challenges for NH3 Oxidation with 100% Conversion and Selectivity. Catalysis Surveys from Asia*, 2021.

26 T. Lan, Y. Zhao, J. Deng, J. Zhang, L. Shi and D. Zhang, Selective catalytic oxidation of NH3 over noble metal-based catalysts: state of the art and future prospects, *Catal. Sci. Technol.*, 2020, **10**(17), 5792–5810.

27 C. K. Lambert, Perspective on SCR NOx control for diesel vehicles, *React. Chem. Eng.*, 2019, **4**(6), 969–974.

28 L. Han, S. Cai, M. Gao, J.-y. Hasegawa, P. Wang, J. Zhang, L. Shi and D. Zhang, Selective Catalytic Reduction of NOx

with NH3 by Using Novel Catalysts: State of the Art and Future Prospects, *Chem. Rev.*, 2019, **119**(19), 10916–10976.

29 L. Chmielarz and M. Jablonska, Advances in selective catalytic oxidation of ammonia to dinitrogen: a review, *RSC Adv.*, 2015, **5**(54), 43408–43431.

30 L. Zhang and H. He, Mechanism of selective catalytic oxidation of ammonia to nitrogen over Ag/Al2O3, *J. Catal.*, 2009, **268**(1), 18–25.

31 L. Gang, B. G. Anderson, J. van Grondelle and R. A. van Santen, Intermediate Species and Reaction Pathways for the Oxidation of Ammonia on Powdered Catalysts, *J. Catal.*, 2001, **199**(1), 107–114.

32 L. Gang, B. G. Anderson, J. van Grondelle and R. A. van Santen, Low temperature selective oxidation of ammonia to nitrogen on silver-based catalysts, *Appl. Catal., B*, 2003, **40**(2), 101–110.

33 J. Martinez-Ortigosa, C. W. Lopes, G. Agostini, A. E. Palomares, T. Blasco and F. Rey, AgY zeolite as catalyst for the selective catalytic oxidation of NH3, *Microporous Mesoporous Mater.*, 2021, **323**, 111230.

34 G. H. Penner and W. Li, Silver-109 NMR Spectroscopy of Inorganic Solids, *Inorg. Chem.*, 2004, **43**(18), 5588–5597.

35 K. Tarach, K. Góra-Marek, M. Chrzan and S. Walas, Quantification of Silver Sites in Zeolites: Carbon Monoxide Sorption Monitored by IR Spectroscopy, *J. Phys. Chem. C*, 2014, **118**(41), 23751–23760.

36 L. Simonelli, C. Marini, W. Olszewski, M. Ávila Pérez, N. Ramanan, G. Guilera, V. Cuartero, K. Klementiev and N. L. Saini, CLAESS: The hard X-ray absorption beamline of the ALBA CELLS synchrotron, *Cogent Phys.*, 2016, **3**(1), 1231987.

37 G. Guilera, F. Rey, J. Hernández-Fenollosa and J. J. Cortés-Vergaz, One body, many heads; the Cerberus of catalysis. a new multipurpose in-situ cell for XAS at ALBA, *J. Phys.: Conf. Ser.*, 2013, **430**, 012057.

38 B. Ravel and M. Newville, ATHENA, ARTEMIS, HEPHAESTUS: data analysis for X-ray absorption spectroscopy using IFEFFIT, *J. Synchrotron Radiat.*, 2005, **12**(Pt 4), 537–541.

39 C. Alonso-Escobar, *Estudio de materiales zeolíticos como estructuras anfitrionas de nanopartículas: aplicaciones catalíticas y medioambientales*, Universitat Politècnica de València, 2017.

40 E. Sayah, D. Brouri and P. Massiani, A comparative *in situ* TEM and UV–visible spectroscopic study of the thermal evolution of Ag species dispersed on Al2O3 and NaX zeolite supports, *Catal. Today*, 2013, **218–219**, 10–17.

41 H. G. Karge and E. Geidel, Vibrational Spectroscopy, in *Characterization I:* –/–, ed. Karge H. G. and Weitkamp J., Springer Berlin Heidelberg, Berlin, Heidelberg, 2004, pp. 1–200.

42 M. Thommes, K. Kaneko, A. V. Neimark, J. P. Olivier, F. Rodriguez-Reinoso, J. Rouquerol and K. S. W. Sing, Physisorption of gases, with special reference to the evaluation of surface area and pore size distribution (IUPAC Technical Report), *Pure Appl. Chem.*, 2015, **87**(9–10), 1051–1069.

